

IMPLEMENTATION OF LOCAL, HIGH-ORDER ACCURATE BOUNDARY CONDITIONS FOR TIME-DEPENDENT ACOUSTIC SCATTERING

Lonny L. Thompson *

Department of Mechanical Engineering
Clemson University
Clemson, South Carolina, 29634
Email: lonny.thompson@ces.clemson.edu

Dantong He and Runnong Huan

Department of Mechanical Engineering
Clemson University
Clemson, South Carolina, 29634

ABSTRACT

A sequence of high-order accurate radiation boundary conditions involving local differential operators of auxiliary functions on a circular boundary are implemented in a spectral finite element method with mixed time integration. The semi-discrete finite element equations are integrated explicitly in time while the auxiliary functions on the circular boundary are integrated using a semi-implicit time-integration method. An efficient algorithm results which avoids the need to update either the solutions for the field variable or the boundary functions at intermediate time steps. Using this mixed time integration approach, a very natural and efficient implementation of the high-order accurate, local boundary conditions is obtained without altering the local/sparse character of the finite element equations. Numerical studies of time-dependent scattering from an elliptic object demonstrate the rapid convergence and accuracy of the implementation.

INTRODUCTION

Hagstrom and Hariharan (Hagstrom,1998) have derived a sequence of high-order accurate radiation boundary conditions involving first-order differential equations in time and tangential derivatives of auxiliary functions on a circular or spherical boundary. In (Thompson,2000; Thompson,1999a; Thompson,1999b), this sequence is reformulated in terms of spherical and Fourier harmonics using a decomposition into orthogonal transverse modes evaluated on spherical and circular boundaries, respectively. In this form, the local boundary conditions

are interpreted as a sequence of residual functions obtained from the hierarchy of local boundary operators used by Bayliss and Turkel (Bayliss,1980) acting on a radial asymptotic (multipole) expansion for outgoing waves. The resulting procedure then involves a Cauchy problem involving systems of first-order temporal equations, similar to that used in (Grote,1995; Thompson,2000). With this reformulation, the auxiliary functions are recognized as residuals of the local boundary operators acting on the asymptotic expansion, and may be implemented efficiently with standard semidiscrete finite element methods without altering the symmetric and sparse structure of the matrix equations. Using harmonics, the method has the ability to vary separately, and up to any desired order, the radial and transverse modal orders of the radiation boundary condition. The primary source of work is the expense in computing the spherical or Fourier transform at each time-step in a time-integration scheme. For a uniform mesh on the radiation boundary, this work may be reduced using the Fast Fourier Transform (FFT). For unstructured meshes, and problems involving a segmented radiation boundary condition, there is motivation to circumvent computation of the harmonic transform and find an efficient method for computing the local conditions directly in physical coordinates.

In this paper, we give an alternate approach which avoids computing the Fourier transform, and directly approximates the sequence of local boundary conditions defined in (Hagstrom,1998) using a spectral finite element method. Numerical experiments in (Hagstrom,1998) for a model problem involving the Fourier modes of the wave equation in two-dimensions indicated the high-order accuracy that can be achieved by directly implementing this sequence of local con-

* Corresponding author.

ditions in a finite difference method. Here we solve the residual functions using a spectral finite element approximation in the angular coordinate on a circular boundary, together with a mixed time integration procedure. The use of spectral elements allows for consistent and high-order approximations for the local boundary conditions within a standard Galerkin variational framework. The interior finite element equations are integrated explicitly in time allowing for efficient parallel computation. Following the suggestion in (Hagstrom,1998) for a finite difference implementation, the spectral element equations for the residual functions on the circular boundary are integrated using a semi-implicit time-integration method. An efficient algorithm results which avoids the need to update either the solutions for the field variable or the residual boundary functions at intermediate time steps. Using this mixed time integration approach, a very natural and efficient implementation of the high-order accurate, local boundary conditions is obtained which allows for the solution to be updated without assembling or factoring finite element matrices. Numerical studies of scattering from an elliptic object demonstrate the rapid convergence and accuracy of the implementation and point to further areas of research.

HELMHOLTZ EQUATION IN EXTERIOR DOMAINS

We consider time-dependent scattering in an infinite two-dimensional region $\mathcal{R} \subset \mathcal{R}^2$, surrounding an object with surface \mathcal{S} . For computation, the unbounded region \mathcal{R} is truncated by a circular boundary Γ , of radius $\|\mathbf{x}\| = R$, see Figure 1. Within

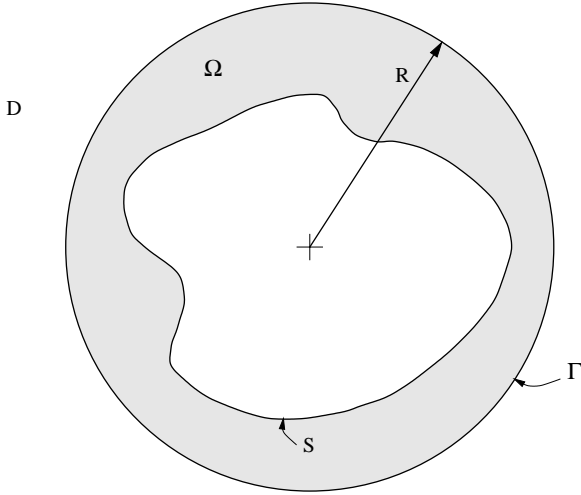


Figure 1. Illustration of unbounded region \mathcal{R} surrounding a scatterer \mathcal{S} . The computational domain $\Omega \subset \mathcal{R}$ is surrounded by a circular truncation boundary Γ of radius R , with exterior region $D = \mathcal{R} - \Omega$.

Ω , the solution $\phi(\mathbf{x}, t) : \Omega \times [0, T] \mapsto \mathcal{R}$, satisfies the scalar wave

equation,

$$\frac{1}{c^2} \frac{\partial^2 \phi}{\partial t^2} = \nabla^2 \phi \quad \mathbf{x} \in \Omega, t \in [0, T] \quad (1)$$

with initial conditions, $\phi(\mathbf{x}, 0) = \phi_o(\mathbf{x})$, $\dot{\phi}(\mathbf{x}, 0) = \dot{\phi}_o(\mathbf{x})$, $\mathbf{x} \in \Omega$, and driven by the time-dependent radiation boundary condition on the surface \mathcal{S} :

$$\frac{\partial \phi}{\partial n} = g(\mathbf{x}, t), \quad \mathbf{x} \in \mathcal{S}, t \in [0, T] \quad (2)$$

In linear acoustics, the scalar function ϕ may represent the pressure field or a velocity potential. The wave speed is assumed $c > 0$, and real. The initial data ϕ_o and $\dot{\phi}_o$ are assumed to be confined to the computational domain Ω , so that in the exterior region $D = \mathcal{R} - \Omega$, i.e., the infinite region outside Γ , the scalar field $\phi(\mathbf{x}, t)$ satisfies the homogeneous form of the wave equation. In polar coordinates (r, θ) , the external region is defined as, $D = \{r \geq R, 0 \leq \theta \leq 2\pi\}$, and the wave equation takes the form,

$$\frac{1}{c^2} \frac{\partial^2 \phi}{\partial t^2} = \frac{\partial^2 \phi}{\partial r^2} + \frac{1}{r} \frac{\partial \phi}{\partial r} + \frac{1}{r^2} \frac{\partial^2 \phi}{\partial \theta^2} \quad (3)$$

The general solution to (3) is given by the Fourier expansion,

$$\phi(r, \theta, t) = \sum_{n=-\infty}^{\infty} \phi_n(r, t) e^{in\theta} \quad (4)$$

For outgoing waves, the time-dependent modes, $\phi_n(r, t)$ may be represented by the radial asymptotic (multipole) expansion:

$$\phi_n(r, t) = \sum_{k=0}^{\infty} r^{-k-1/2} \phi_n^k(r-ct) \quad (5)$$

with wave functions satisfying the following recursion relation (Hagstrom,1998; Thompson,1999a; Thompson,1999b),

$$\left(\phi_n^k\right)' = \frac{(k-1/2)^2 - n^2}{2k} \phi_n^{k-1}, \quad k = 1, 2, \dots, n \quad (6)$$

LOCAL RADIATION BOUNDARY CONDITIONS

In (Thompson,1999a; Thompson,1999b), the local radiation boundary conditions first derived in (Hagstrom,1998) are formulated using the well-known hierarchy of local operators given in (Bayliss,1980),

$$B_p = L_p(L_{p-1}(\dots(L_2(L_1)))) \quad (7)$$

$$L_j = \left(\frac{1}{c} \frac{\partial}{\partial t} + \frac{\partial}{\partial r} + \frac{2j-3/2}{r} \right). \quad (8)$$

In this approach, the residuals of the operators (8) acting on the asymptotic expansion (5) are interpreted as a sequence of functions with reduced radial order. Applying $B_1 = L_1$ to the radial expansion (5), results in the following residual (Thompson,1999a; Thompson,1999b),

$$B_1 \phi_n = \left(\frac{1}{c} \frac{\partial}{\partial t} + \frac{\partial}{\partial r} + \frac{1}{2r} \right) \phi_n(r,t) = w_n^1(r,t) \quad (9)$$

$$w_n^1(r,t) = \sum_{k=1}^{\infty} -k r^{-k-3/2} \phi_n^k \quad (10)$$

The function w_{nm}^1 defines the remainder of the radial expansion, with error $O(R^{-5/2})$ for $n \geq 2$. In general, applying B_{j+1} to (5), results in

$$B_{j+1} \phi_n = L_{j+1}(w_n^j) = \left(\frac{1}{c} \frac{\partial}{\partial t} + \frac{\partial}{\partial r} + \frac{2j+1/2}{r} \right) w_n^j = w_n^{j+1} \quad (11)$$

where the residual of B_j is defined as,

$$w_n^j(r,t) = \sum_{k=j}^{\infty} a_k^j r^{-k-j-1/2} \phi_n^k, \quad a_k^j = (-1)^j \frac{k!}{(k-j)!}. \quad (12)$$

The important observation here is that the order of the residuals are reduced significantly to $w_n^{j+1} = O(r^{-2})w_n^j$, $w_n^j(r,t) = O(r^{-2j-1/2})$. Using the recursion relation for $(\phi_n^k)'$ given in (6), and the definition for a_k^j , the radial derivatives in (11) may be eliminated in favor of a recursive sequence for $y_n^j(r,t) = 2^{1-j}w_n^j$, with the result (Thompson,1999a; Thompson,1999b),

$$\frac{1}{c} \frac{\partial y_n^j}{\partial t} = \frac{1}{4r^2} \left[\left(j - \frac{1}{2} \right)^2 - n^2 \right] y_n^{j-1} - \frac{j}{r} y_n^j + y_n^{j+1} \quad (13)$$

for $j = 1, 2, \dots, p$, and $y_n^0 = 2\phi_n$. Applying the Fourier expansion to (9) and (13), evaluated at $r = R$, and making use of the eigenvalues $-n^2$ for the exponential, results in the radiation condition, defined by the sequence of local operators,

$$\left(\frac{1}{c} \frac{\partial}{\partial t} + \frac{\partial}{\partial r} + \frac{1}{2R} \right) \phi = v_1(\theta, t) \quad (14)$$

$$\left(\frac{1}{c} \frac{\partial}{\partial t} + \frac{j}{R} \right) v_j = \frac{1}{4R^2} \left[\left(j - \frac{1}{2} \right)^2 + \frac{\partial^2}{\partial \theta^2} \right] v_{j-1} + v_{j+1} \quad (15)$$

where

$$v_j(\theta, t) = \sum_{n=-\infty}^{\infty} y_n^j(R, t) e^{in\theta} \quad (16)$$

for $j = 1, 2, \dots, p$, and $v_0 = 2\phi, v_{p+1} = 0$. The local radiation condition (14), together with the sequence of p equations (15), defines the local conditions first derived by Hagstrom and Hariharan in (Hagstrom,1998).

In (Thompson,1999a; Thompson,1999b), this sequence is reformulated in terms of Fourier harmonics evaluated on the artificial boundary at $r = R$. In this approach the sequence (13) forms a system of first-order ordinary differential equations in time for the auxiliary functions, $v_n^j(t) = y_n^j(R, t)$, and driven by the radial modes,

$$\phi_n(R, t) = \frac{1}{2\pi} \int_0^{2\pi} e^{-in\theta} \phi(R, \theta, t) d\theta. \quad (17)$$

Using Fourier harmonics, the method has the ability to vary separately, and up to any desired order, the radial and transverse modal orders of the radiation boundary condition. The resulting procedure then involves a Cauchy problem involving systems of first-order temporal equations, similar to that used in (Grote,1995; Thompson,2000). The decomposition into orthogonal transverse modes on the circular boundary allows the residual functions to be computed efficiently and concurrently without altering in any way the symmetric, sparse structure of the semi-discrete finite element matrix equations in the interior region Ω . The primary source of work is the expense in computing the Fourier transform (17) at each time-step. For a uniform mesh on Γ , this work may be reduced using the Fast Fourier Transform (FFT). For unstructured meshes, there is motivation to circumvent computation of the inner-products of finite element basis functions with trigonometric functions implied by (17).

In this paper, we give an alternate approach which avoids computing the Fourier transform, and directly approximates the sequence of local boundary conditions defined in (14) and (15) using a spectral finite element method. Here we solve the auxiliary functions $v_j(\theta, t)$, using a spectral finite element approximation in the angular coordinate θ , together with a mixed time integration procedure. The interior finite element equations in Ω are integrated explicitly in time while the auxiliary functions on the circular boundary Γ are integrated using a semi-implicit time-integration method. An efficient algorithm results which avoids the need to update either the solutions for the field variable ϕ , or the auxiliary boundary functions v_j , at intermediate time steps.

Using this mixed time integration approach, a very natural and efficient implementation of the high-order accurate, local boundary conditions is obtained which allows for both ϕ and v_j to be updated without assembling or factoring finite element matrices.

Let $\mathbf{v}(\theta, t) = \{v_j(\theta, t)\}$, $j = 1, 2, \dots, p$, be defined as a time-dependent vector of order p ,

$$\mathbf{v} = [v_1, v_2, \dots, v_p]^T \quad (18)$$

then the sequence (15) may be formulated as a coupled system of first-order partial differential equations in matrix form:

$$\frac{1}{c} \frac{\partial \mathbf{v}}{\partial t} = \mathbf{A} \mathbf{v} + \mathbf{b} \phi(R, \theta, t) \quad (19)$$

Here, the constant $p \times p$, tri-diagonal matrix $\mathbf{A} = \{A_{ij}\}$, may be split in two parts,

$$\mathbf{A} = \mathbf{A}_1 + \mathbf{A}_2 \frac{\partial^2}{\partial \theta^2} \quad (20)$$

with \mathbf{A}_1 and \mathbf{A}_2 defined with band:

$$\mathbf{A}_1 = \frac{1}{R} \mathbf{B} \left[\frac{1}{4R} (j - \frac{1}{2})^2, -j, R \right] \quad (21)$$

$$\mathbf{A}_2 = \frac{1}{4R^2} \mathbf{B} [1, 0, 0] \quad (22)$$

Similarly, the constant vector $\mathbf{b} = \{b_j\}$ is split as,

$$\mathbf{b} = \mathbf{b}_1 + \mathbf{b}_2 \frac{\partial^2}{\partial \theta^2} \quad (23)$$

$$\mathbf{b}_1 = \frac{1}{8R^2} [1, 0, \dots, 0]^T \quad (24)$$

$$\mathbf{b}_2 = \frac{1}{2R^2} [1, 0, \dots, 0]^T \quad (25)$$

Due to the rapid convergence of the functions v_j , for accurate solutions, it is sufficient to use only few auxiliary functions on Γ .

FINITE ELEMENT FORMULATION

A variational equation is obtained by multiplying (19) with a weighting function $\delta \mathbf{v}^T$, integrating over the circular boundary

Γ , and using the periodic conditions $\mathbf{v}(0, t) = \mathbf{v}(2\pi, t)$, with the result,

$$\frac{1}{c} (\delta \mathbf{v}, \frac{\partial \mathbf{v}}{\partial t})_{\Gamma} = K_v (\delta \mathbf{v}, \mathbf{v}) + F_v (\delta \mathbf{w}, \phi) \quad (26)$$

$$(\delta \mathbf{v}, \mathbf{v})_{\Gamma} := \int_{\Gamma} \delta \mathbf{v}^T \mathbf{v} d\Gamma \quad (27)$$

$$K_v (\delta \mathbf{v}, \mathbf{v}) := \int_{\Gamma} \delta \mathbf{v}^T \mathbf{A}_1 \mathbf{v} d\Gamma - \int_{\Gamma} \frac{\partial \delta \mathbf{v}^T}{\partial \theta} \mathbf{A}_2 \frac{\partial \mathbf{v}}{\partial \theta} d\Gamma \quad (28)$$

$$F_v (\delta \mathbf{v}, \phi) := \int_{\Gamma} \delta \mathbf{v}^T \mathbf{b}_1 \phi d\Gamma - \int_{\Gamma} \frac{\partial \delta \mathbf{v}^T}{\partial \theta} \mathbf{b}_2 \frac{\partial \phi}{\partial \theta} d\Gamma \quad (29)$$

Similarly, multiplying the wave equation (1) by the weighting function $\delta \phi$, integrating over the interior domain Ω using the divergence theorem, and incorporating the local radiation condition (14) evaluated on the circular boundary at $r = R$, gives the coupled equation,

$$(\delta \phi, \frac{1}{c^2} \frac{\partial^2 \phi}{\partial t^2})_{\Omega} + (\delta \phi, \frac{1}{c} \frac{\partial \phi}{\partial t})_{\Gamma} + K_{\phi} (\delta \phi, \phi) = F_{\phi} (\delta \phi, v_1) \quad (30)$$

$$K_{\phi} (\delta \phi, \phi) := \int_{\Omega} \nabla \delta \phi \cdot \nabla \phi d\Omega + \frac{1}{2R} \int_{\Gamma} \delta \phi \phi d\Gamma \quad (31)$$

$$F_{\phi} (\delta \phi, v_1) := \int_S \delta \phi g dS + \int_{\Gamma} \delta \phi v_1 d\Gamma \quad (32)$$

For the interior finite element equations in Ω , we use a standard Galerkin semi-discrete approximation, $\phi(\mathbf{x}, t) \approx \phi^h(\mathbf{x}, t) = \mathbf{N}(\mathbf{x}) \boldsymbol{\phi}(t)$. This leads to the coupled system of second-order ordinary differential equations in time:

$$\mathbf{M}_{\phi} \ddot{\boldsymbol{\phi}}(t) + \mathbf{C}_{\phi} \dot{\boldsymbol{\phi}}(t) + \mathbf{K}_{\phi} \boldsymbol{\phi}(t) = \mathbf{F}_{\phi}(t), \quad t > 0 \quad (33)$$

In the above, \mathbf{M}_{ϕ} , \mathbf{C}_{ϕ} , and \mathbf{K}_{ϕ} are standard arrays associated with the discretization of the wave equation and the local B_1 operator; and $\mathbf{F}_{\phi}(t)$ is the discrete force vector composed of a standard load vector and a part associated with the auxiliary function v_1 ,

$$\mathbf{F}_{\phi}(t) = \int_{\Gamma} \mathbf{N}_{\phi}^T v_1 d\Gamma \quad (34)$$

The function v_1 is the first element of the vector array $\mathbf{v} = \{v_j\}$, which satisfies the coupled system (26) driven by $\phi(R, \theta, t)$.

Let $\mathbf{F}_\phi^k = \mathbf{F}_\phi(t_k)$ be the force at time step $t_k = k\Delta t$. Here, we compute the solution $\phi^{k+1} = \phi(t_{k+1})$, by applying the second-order accurate, *explicit* central difference method to the interior finite element matrix equations given in (33), with the result:

$$\hat{\mathbf{M}}\phi^{k+1} = \mathbf{R}^k \quad (35)$$

with effective mass matrix,

$$\hat{\mathbf{M}} = \frac{1}{\Delta t^2}\mathbf{M}_\phi + \frac{1}{2\Delta t}\mathbf{C}_\phi \quad (36)$$

and

$$\mathbf{R}^k = \mathbf{F}_\phi^k - \left(\mathbf{K}_\phi - \frac{2}{\Delta t^2}\mathbf{M}_\phi\right)\phi^k - \left(\frac{1}{\Delta t^2}\mathbf{M}_\phi - \frac{1}{2\Delta t}\mathbf{C}_\phi\right)\phi^{k-1} \quad (37)$$

The algebraic equations given in (35) are decoupled using a spectral element method with nodal (Gauss-Lobatto) quadrature to diagonalize \mathbf{M}_ϕ and \mathbf{C}_ϕ . With a diagonal effective mass $\hat{\mathbf{M}}$, the system of equations (35) can be solved without factorizing a matrix; i.e., only matrix multiplications are required to obtain the right-hand-side effective load vector \mathbf{R}^k , after which the nodal solutions ϕ_n can be updated using,

$$\phi_n^{k+1} = \frac{R_n^k}{\hat{m}_{nn}} \quad (38)$$

where ϕ_n^{k+1} and R_n^k denote the n th components of the vectors ϕ^{k+1} and \mathbf{R}^k , respectively, and \hat{m}_{nn} is the n th diagonal element of the effective mass matrix obtained from the lumped mass and damping matrices. Furthermore, the matrix-vector product $\mathbf{K}_\phi\phi^k$ can be evaluated at the element level by summing the contributions from each element to the effective load vector, without matrix assembly of \mathbf{K}_ϕ , rendering a highly efficient algorithm suitable for parallel implementation for large-scale analysis.

For the auxiliary functions we use a consistent spectral element approximation on the boundary Γ , with nodal (Gauss-Lobatto) quadrature (Thompson,1994). At the element level we approximate $\mathbf{v}(\theta, t)$, using Lagrange interpolation basis functions N_i^e , of order q , associated with nodes i , positioned at Gauss-Lobatto quadrature points,

$$\mathbf{v}(\theta, t) = \sum_{i=1}^{q+1} N_i^e(\theta)\mathbf{v}_i^e(t), \quad \theta \in \Gamma_e = [\theta_1^e, \theta_{q+1}^e]. \quad (39)$$

In the above, $\mathbf{v}_i^e(t) = \mathbf{v}(\theta_i^e, t)$. Arranging the nodal functions in vector form $\mathbf{d}_v^e(t) = [\mathbf{v}_1^e, \mathbf{v}_2^e, \dots, \mathbf{v}_{q+1}^e]^T$, we have $\mathbf{v} = \mathbf{N}_v^{eT} \mathbf{d}_v^e$,

where \mathbf{N}_v^e is an array of shape functions for an element on Γ . Using this approximation in (26) leads to the matrix system,

$$\mathbf{C}_v \dot{\mathbf{d}}_v(t) = \mathbf{K}_v \mathbf{d}_v(t) + \mathbf{F}_v(t), \quad t > 0 \quad (40)$$

$$\mathbf{C}_v := \bigwedge_{e=1}^{N_{\Gamma_e}} \frac{1}{c} \int_{\Gamma_e} \mathbf{N}_v^{eT} \mathbf{N}_v R d\theta \quad (41)$$

$$\mathbf{K}_v := \bigwedge_{e=1}^{N_{\Gamma_e}} \left\{ \int_{\Gamma_e} \mathbf{N}_v^{eT} \mathbf{A}_1 \mathbf{N}_v R d\theta - \int_{\Gamma_e} \mathbf{N}_{v,\theta}^{eT} \mathbf{A}_2 \mathbf{N}_{v,\theta} R d\theta \right\} \quad (42)$$

$$\mathbf{F}_v := \bigwedge_{e=1}^{N_{\Gamma_e}} \left\{ \int_{\Gamma_e} \mathbf{N}_v^{eT} \mathbf{b}_1 \phi R d\theta - \int_{\Gamma_e} \mathbf{N}_{v,\theta}^{eT} \mathbf{b}_2 \phi_{,\theta} R d\theta \right\} \quad (43)$$

In the above, $\bigwedge_{e=1}^{N_{\Gamma_e}}$ is the assembly (gather) operation for the number of elements on the boundary Γ , and \mathbf{d}_v is the global DOF vector of dimension $N_\Gamma \times p$, where N_Γ is the total number of nodes on the boundary Γ , and p is the number of auxiliary functions included in the sequence of boundary operators. These integrals may be preintegrated and assembled in closed-form. For example, for the case of linear interpolation functions with $q = 1$, and using nodal quadrature on a nonuniform mesh, we have the assembled arrays in block tridiagonal form associated with nodal matrix partitions,

$$\mathbf{C}_v = \frac{R}{2c} \mathbf{B}[\mathbf{0}, (\Delta\theta_n + \Delta\theta_{n-1})\mathbf{I}_p, \mathbf{0}] \quad (44)$$

$$\mathbf{K}_v = \mathbf{K}_v^1 + \mathbf{K}_v^2 \quad (45)$$

$$\mathbf{K}_v^1 = \frac{R}{2} \mathbf{B}[\mathbf{0}, (\Delta\theta_n + \Delta\theta_{n-1})\mathbf{A}_1, \mathbf{0}] \quad (46)$$

$$\mathbf{K}_v^2 = R \mathbf{B}[\frac{1}{\Delta\theta_{n-1}}\mathbf{A}_2, -\left(\frac{1}{\Delta\theta_n} + \frac{1}{\Delta\theta_{n-1}}\right)\mathbf{A}_2, \frac{1}{\Delta\theta_{n-1}}\mathbf{A}_2] \quad (47)$$

where $\Delta\theta_n = \theta_{n+1} - \theta_n = \theta_2^e - \theta_1^e$, $n = 1, 2, \dots, N_\Gamma$, and \mathbf{I}_p is the identity matrix with dimension $p \times p$. For a full circular boundary the matrix \mathbf{K}_v^2 has an additional block $\mathbf{A}_2/\Delta\theta_{N_\Gamma}$ in the corners due to the periodic conditions.

The nodal partition for the coupling vector $\mathbf{F}_v = \mathbf{F}_v^1 + \mathbf{F}_v^2$, can be written in closed form as,

$$\{\mathbf{F}_v^1\}_n = \phi_n (\Delta\theta_n + \Delta\theta_{n-1}) \frac{R}{2} \mathbf{b}_1, \quad (48)$$

$$\{\mathbf{F}_v^2\}_n = \frac{(\phi_{n+1} - \phi_n)}{\Delta\theta_n} R \mathbf{b}_2 - \frac{(\phi_n - \phi_{n-1})}{\Delta\theta_{n-1}} R \mathbf{b}_2, \quad (49)$$

for $n = 1, 2, \dots, N_\Gamma$, and $\Delta\theta_0 = \Delta\theta_{N_\Gamma}$.

Following the suggestion in (Hagstrom, 1998), we formulate a semi-implicit time-integration scheme for the auxiliary equations. To this end, we split the matrix,

$$K_v = \mathbf{L} + \mathbf{U}, \quad (50)$$

into a lower triangle including diagonal part \mathbf{L} , and a strictly upper triangle part \mathbf{U} . The upper triangle part \mathbf{U} , is treated explicitly using the second-order accurate Adams-Bashford method, while the remaining terms are integrated with the implicit trapezoidal rule. To advance the solution $\mathbf{d}_v^{k+1} = \mathbf{d}_v(t_{k+1})$, we compute

$$\hat{\mathbf{L}}\mathbf{d}_v^{k+1} = \left(\mathbf{C}_v + \frac{\Delta t}{2}(\mathbf{L} + 3\mathbf{U}) \right) \mathbf{d}_v^k - \frac{\Delta t}{2}\mathbf{U}\mathbf{d}_v^{k-1} + \mathbf{F}_v^{k+1/2} \quad (51)$$

with the modified lower triangle matrix and average force,

$$\hat{\mathbf{L}} = \mathbf{C}_v - \frac{\Delta t}{2}\mathbf{L} \quad (52)$$

$$\mathbf{F}_v^{k+1/2} = \frac{\Delta t}{2} \left(\mathbf{F}_v^k + \mathbf{F}_v^{k+1} \right) \quad (53)$$

Using this semi-implicit splitting, the system (51) is solved in sequence using a simple forward sweep over nodal blocks $n = 1, 2, \dots, N_\Gamma$. In two-dimensions, further efficiency is gained by utilizing the closed-form difference stencil for the j th row of the matrix partition associated with a typical node n . Let $\gamma = c\Delta t/2R$, then using the block matrix structure given described earlier, the space-time stencil associated with the j th auxiliary function at node n , denoted $(v_j)_n$, is given by,

$$\begin{aligned} [1 + j\gamma](v_j)_n^{k+1} &= [1 - j\gamma](v_j)_n^k \\ &+ \gamma R [3(v_{j+1})_n^k - (v_{j+1})_n^{k-1}] \\ &+ \frac{\gamma}{4R} \left[\left(j - \frac{1}{2} \right)^2 + \delta^2 \right] [(v_{j-1})_n^{k+1} + (v_{j-1})_n^k]. \\ n &= 1, 2, \dots, N_\Gamma, \quad j = 1, 2, \dots, p. \\ (v_0)_n &= 2\phi_n, \quad (v_{p+1})_n = 0 \end{aligned} \quad (54)$$

In the above, δ^2 is defined by the second-order spatial difference operator on a nonuniform grid,

$$\delta^2(v_j)_n = \frac{1}{\alpha_n^2} [\beta_n(v_j)_{n-1} - (1 + \beta_n)(v_j)_n + (v_j)_{n+1}] \quad (55)$$

$$\frac{1}{\alpha_n^2} := \frac{2}{\beta_n(1 + \beta_n)\Delta\theta_{n-1}^2}, \quad \beta_n = \Delta\theta_n/\Delta\theta_{n-1} \quad (56)$$

Using this stencil, the solution for the auxiliary functions $(v_j)_n^{k+1}$ is advanced efficiently in sequence for $j = 1, 2, \dots, p$, and node $n = 1, 2, \dots, N_\Gamma$, without matrix assembly or matrix factorization. We note, that this stencil can also be obtained directly from a second-order finite difference approximation of the sequence of local boundary conditions in differential form (15). However, through the use of the spectral element formulation with closed form and symbolic matrix integration/assembly procedures described here, high-order accurate approximations (quadratic, cubic, etc.) are derived which are *consistent* with the finite element method used for the interior field variable. Using this approach, consistent and high-order accurate space-time difference stencils on nonuniform grids may be derived similar to (54).

After initial conditions are established, the complete coupled time-integration algorithm proceeds as follows:

- (1) calculate the effective load at time t from (37),
- (2) update the field solution at time $t + \Delta t$ from (38),
- (3) solve for the auxiliary functions $(v_j)_n$ at time $t + \Delta t$ from (54) in sequence for $j = 1, 2, \dots, p$, and $n = 1, 2, \dots, N_\Gamma$,
- (4) update the time step, and repeat.

The key to the effectiveness of this algorithm is that the field update relies only on the auxiliary functions at the current time step, i.e., \mathbf{v}^k ; and the update of the auxiliary functions relies only on the most recently computed solution ϕ^{k+1} at time step t_{k+1} . The result is a very natural algorithm which avoids the need for intermediate updates between equations as would be the case in a staggered-step time integration.

In three-dimensions, a stencil similar to (54) can be written for orthogonal grids on a sphere. For general unstructured meshes, as would be generated using an automatic free mesh algorithm, the system can still be solved efficiently using a forward sweep of the matrix system (51).

NUMERICAL STUDIES

Consider the problem of time-dependent scattering from an elliptic cylinder. The ellipse is defined by coordinates $x = f \cosh \mu \cos \theta$, and $y = f \sinh \mu \sin \theta$. Here we choose the radial coordinate $\mu_0 = 0.2$, and foci $f = 1$, resulting in an aspect ratio of major to minor axis of approximately 5 : 1. The cylinder is assumed infinite in the z -direction, so that the problem can be solved as a two-dimensional problem in the xy -plane.

On the surface of the cylinder, we assume a 'soft' (homogeneous Dirichlet) boundary condition,

$$\phi = \phi^{(i)} + \phi^{(s)} = 0, \quad \text{on } \mathcal{S} := \{\mu_0 = 0.1, 0 \leq \theta \leq 2\pi\} \quad (57)$$

Here the total field $\phi(\mu, \theta)$ is composed of the incident wave $\phi^{(i)}$, and the scattered wave field $\phi^{(s)}$, such that $\phi^{(s)}(\mu_0, \theta) = -\phi^{(i)}(\mu_0, \theta)$.

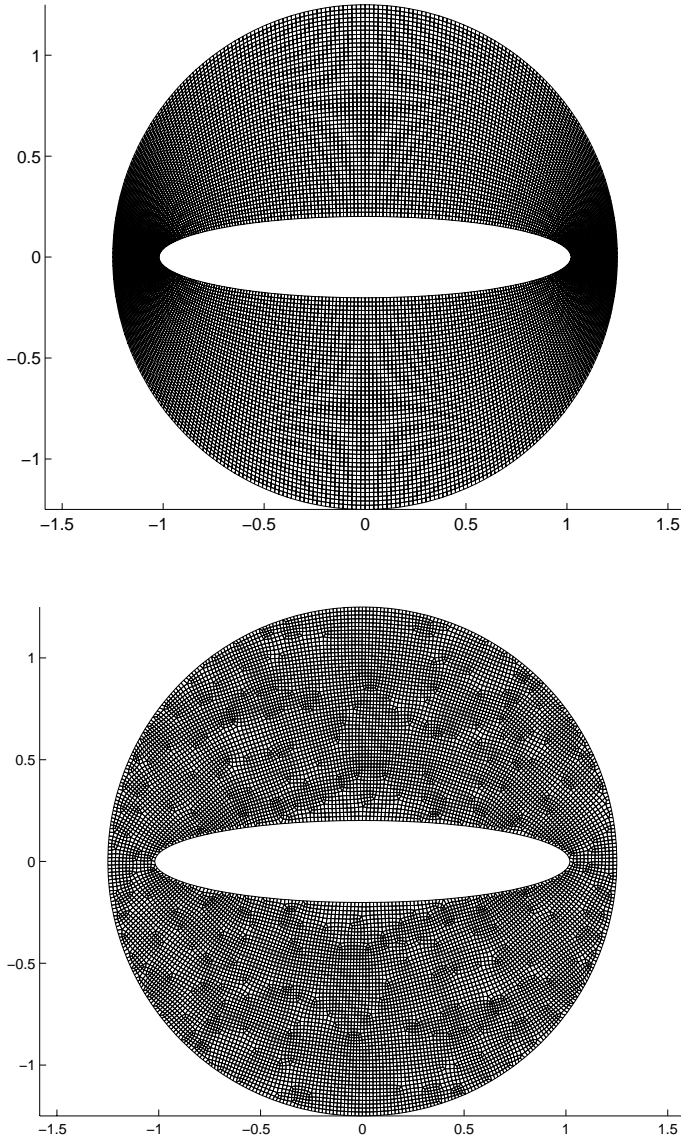


Figure 2. Finite element mesh for elliptic scatterer defined with foci $f = 1$, $\mu = 0.2$. The circular radiation boundary Γ , is positioned at $R = 1.25$. (Top) Uniform mesh (Mesh1), (Bottom) Unstructured mesh (Mesh2).

The incident plane-wave is given by,

$$\phi^{(i)}(\mathbf{x}, t) = \sin[k\mathbf{v} \cdot (\mathbf{x} - \mathbf{x}_0) - \omega t] H[t - \mathbf{v} \cdot (\mathbf{x} - \mathbf{x}_0)/c] \quad (58)$$

Here $\mathbf{x}_0 = [x_0, y_0]$ defines the position of the initial wave front at $t = 0$. The direction of the incident plane-wave is determined by the unit wave vector $\mathbf{v} = [\cos \alpha, \sin \alpha]$, where α is the angle between the lines of constant phase and the x -axis.

We obtain the exact steady-state solution for the scattered field by expanding the exponential form of the incident

wave in elliptic coordinates by means of an addition theorem (Morse, 1953). For $\phi^{(i)}$ given in (58), and homogeneous boundary condition (57), the steady-state analytical solution is,

$$\phi^{(s)}(\mu, \theta, t) = \text{Imag} \left\{ \hat{\phi}^{(s)}(\mu, \theta) e^{-i(k\mathbf{v} \cdot \mathbf{x}_0 + \omega t)} \right\} \quad (59)$$

where

$$\hat{\phi}^{(s)}(\mu, \theta) = -2 \sum_{n=0}^{\infty} i^n \left\{ A_n M C_n^{(3)}(\mu, q) c e_n(\theta, q) + B_n M S_n^{(3)}(\mu, q) s e_n(\theta, q) \right\} \quad (60)$$

$$A_n = \frac{M C_n^{(1)}(\mu_0, q)}{M C_n^{(3)}(\mu_0, q)} c e_n(\alpha, q) \quad (61)$$

$$B_n = \frac{M S_n^{(1)}(\mu_0, q)}{M S_n^{(3)}(\mu_0, q)} s e_n(\alpha, q) \quad (62)$$

In the above, $q = (kf/2)^2$, $c e_n$ and $s e_n$ are the even and odd valued angular Mathieu functions, and $M C_n^{(p)}$ and $M S_n^{(p)}$, $p = 1, 3$ are even and odd radial (modified) Mathieu functions of the first and third kind, respectively (Abramowitz, 1968).

For the finite element solution, the radius of the circular radiation boundary Γ is set at $R = 1.25$. The numerical solution for this scattering problem is solved using a total field method similar to that described in (Thompson, 2000), here formulated for the two-dimensional problem. We use 3 different finite element meshes. In the first (Mesh1), the computational domain is discretized with a quasi-uniform mesh of standard 4-node bilinear finite elements with $N_\Gamma = 360$ evenly spaced node points on the circular radiation boundary Γ , and 50 node points in the radial direction, resulting in $N_T = 18,360$ total nodes and elements, see Figure 2. The other two meshes considered are unstructured meshes generated using the ‘free mesh’ option in the CAE software package I-DEAS from SDRC. The first unstructured mesh (Mesh2) uses an average element length of $h = 0.018$, resulting in $N_T = 16,205$ nodes with $N_S = 236$ nonuniform boundary nodes on the inner ellipse, and $N_\Gamma = 436$ nodes on the outer radiation boundary. The second unstructured mesh (Mesh3) uses a finer grid with an average element length $h = 0.012$, resulting in $N_T = 35,906$, $N_S = 354$, and $N_\Gamma = 654$ nonuniform nodes. The computation is driven from rest to steady-state with wave vector angle $\alpha = 30^\circ$, and frequency $k = \omega/c = 2\pi$. The initial wave front starts at the radiation boundary, such that $\mathbf{x}_0 = -R\mathbf{v}$.

In the following we denote by $\text{LBC}(p)$, the spectral element approximation to the sequence of local radiation boundary operators defined in (14) and (15), where p is the number

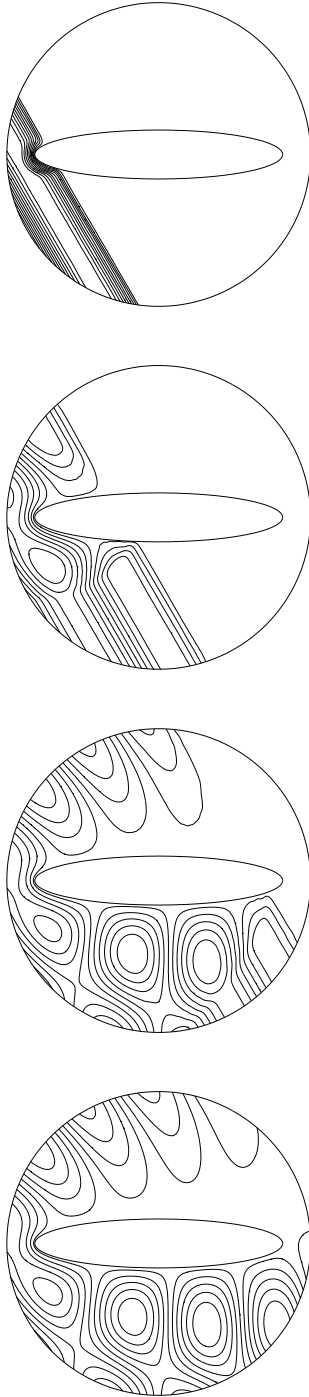


Figure 3. Scattering from an elliptic cylinder with incident plane-wave oriented in $\theta = 30^\circ$ direction, and normalized frequency $k = \omega/c = 2\pi$. Finite element solution contours for the *total field* at snapshots in time.

of residual functions included. Figures 3 and 4 show finite element solution contours for both total and scattered fields at time $t = (0.5, 1.0, 2.0, 5.0)$, using the sequence of local radiation boundary conditions LBC(10), with $p = 10$ auxiliary functions. At $t = 0.5$, the incident plane-wave has just begun to diffract from the elliptic cylinder. At $t = 5.0$, the solution has nearly reached steady-state.

Figure 5 shows the maximum L_2 error using LBC(p) and the semi-implicit time-integration scheme described in (51) and (54), and using different time steps, denoted $A4(\Delta t)$. The results are compared with the implementation RBC1(N, p) given in (Thompson,1999a; Thompson,1999b), with $N = 20$ angular harmonics included in the Fourier expansion, and the explicit time integration algorithm described in (Thompson,2000), denoted $A2(\Delta t)$. The results show that using the local radiation conditions, the error decreases rapidly, with only $p = 4$ residual functions needed to converge to a fixed lower bound. The fixed lower error bound is primarily controlled by the explicit space-time discretization of the wave equation in the interior field; as the time-step is decreased the lower-bound decreases accordingly. Accuracy of the direct implementation of the local operators given in this paper matches the accuracy of the indirect implementation using a Fourier expansion with $N = 20$ angular harmonics as described in (Thompson,1999a; Thompson,1999b). This result is expected since both methods are based on the same radial expansion (5) with p residual functions. For very high-orders $p > 16$, we observe that the semi-implicit time-integration scheme becomes unstable. This instability is also shown using the unstructured meshes shown in Figure 6. As the mesh is refined the instability appears at the lower order of $p = 12$. These results show that the semi-implicit scheme for the auxiliary conditions, while extremely efficient, is only conditionally stable and is sensitive to space-time discretization and radial order p . Fortunately, due to the rapid convergence of the residual functions in the boundary conditions, only a low-order value p is required, leading to an accurate and stable solution for this problem. These results motivate the investigation of an efficient implicit and unconditionally stable time-integration scheme for direct implementation for the sequence of local boundary conditions. Preliminary work on taking advantage of the nodal block structure of the auxiliary equations in an implicit framework shows promise for efficient time-integration and will be reported in a forthcoming paper.

CONCLUSIONS

Asymptotic local radiation boundary conditions first derived by Hagstrom and Hariharan for the time-dependent wave equation, are formulated in a high-order accurate spectral element method with mixed time-integration. Using this mixed time integration approach, a very natural implementation of the high-order accurate, local boundary conditions is obtained which allows the boundary conditions to be implemented efficiently with-

out altering the local character of the finite element equations. By using a semi-implicit time-integration method for the boundary matrices, an efficient solution is obtained using a forward sweep on a lower triangle matrix, without factoring finite element matrices. Further efficiency is gained by recognizing the nodal block structure of the auxiliary equations to form consistent space-time difference stencils on a nonuniform boundary mesh. Using this stencil, the auxiliary functions can be updated in time, and in sequence for each node on the radiation boundary, without matrix assembly. Extensions to three-dimensions for unstructured meshes on a sphere follow directly from the methods described here for the two-dimensional case. Numerical studies of scattering from an elliptic object demonstrate that the accuracy rapidly converges with the number of residual functions included in the sequence. The accuracy matches the alternative implementation using Fourier harmonics, as expected, without computing Fourier transforms. The semi-implicit time-integration scheme is conditionally stable and sensitive to space-time discretization and the radial order used in the sequence of local boundary operators. At very high radial orders, the semi-implicit method may become unstable, motivating the efficient implementation of an unconditionally stable implicit scheme.

ACKNOWLEDGMENT

Support for this work was provided by the National Science Foundation under Grant CMS-9702082 in conjunction with a Presidential Early Career Award for Scientists and Engineers (PECASE), and is gratefully acknowledged.

REFERENCES

- T. Hagstrom and S. Hariharan, 'A formulation of asymptotic and exact boundary conditions using local operators', *Appl. Num. Math.* **27**, 403-416, 1998.
- A. Bayliss and E. Turkel, 'Radiation boundary conditions for wave-like equations', *Commun. Pure Appl. Math.*, **33**, 707-725, 1980.
- M. J. Grote and J. B. Keller, 'Exact non-reflecting boundary conditions for the time dependent wave equation', *SIAM J. of Appl. Math.*, **55** (1995), pp. 280-297.
- L. L. Thompson and R. Huan, 'Implementation of Exact Non-Reflecting Boundary Conditions in the Finite Element Method for the Time-Dependent Wave Equation', *Computer Methods in Applied Mechanics and Engineering*, **187**, 1-2 (2000) pp. 137-159.
- R. Huan and L.L. Thompson, 'Accurate radiation boundary conditions for the time-dependent wave equation on unbounded domains', *I. J. for Numerical Methods in Engineering*, **47**, pp. 1569-1603, (2000).
- L.L.Thompson and R. Huan and D. He, 'Accurate radiation boundary conditions for the two-dimensional wave equation on

unbounded domains', *Computer Methods in Applied Mechanics and Engineering*, Accepted in principle with revision.

L.L.Thompson and R. Huan, 'Asymptotic and Exact Radiation Boundary Conditions for Time-Dependent Scattering', *Proceedings of the ASME Noise Control and Acoustics Division - 1999 ASME 1999 International Mechanical Engineering Congress and Exposition, NCA-Vol. 26, Symposium on Computational Acoustics*, pp. 511-521, Nashville, TN, Nov. 14-19, 1999.

Thompson, L.L., and Pinsky, P.M., 'Complex wavenumber Fourier analysis of the p-version finite element method', *Journal of Computational Mechanics*, **13**, (4), pp. 255-275, 1994.

P.M. Morse and H. Feshbach, *Methods of Theoretical Physics*, McGraw-Hill, 1953.

M. Abramowitz and I. Stegun, Eds., *Handbook of Mathematical Functions*, Washington, DC: National Bureau of Standards, 1964. Reprinted by Dover Publications, New York, 1968, pp. 751-770.

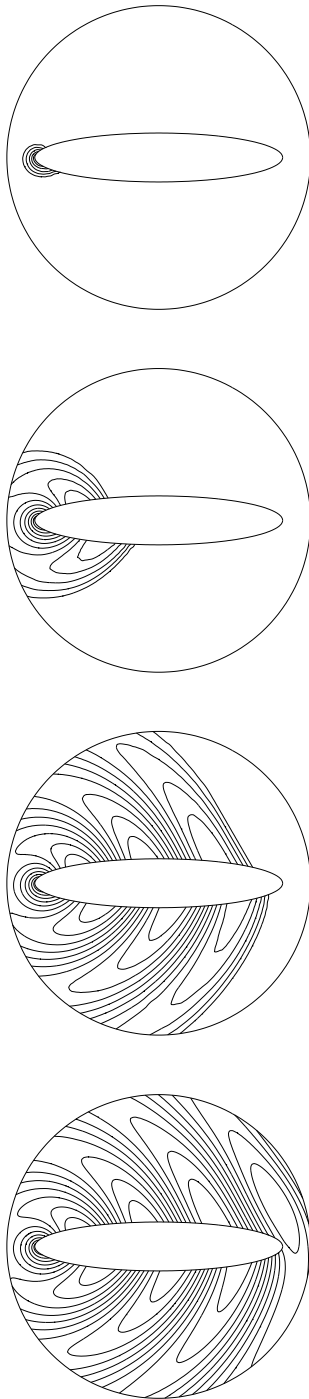


Figure 4. Finite element solution contours for the *scattered field*.

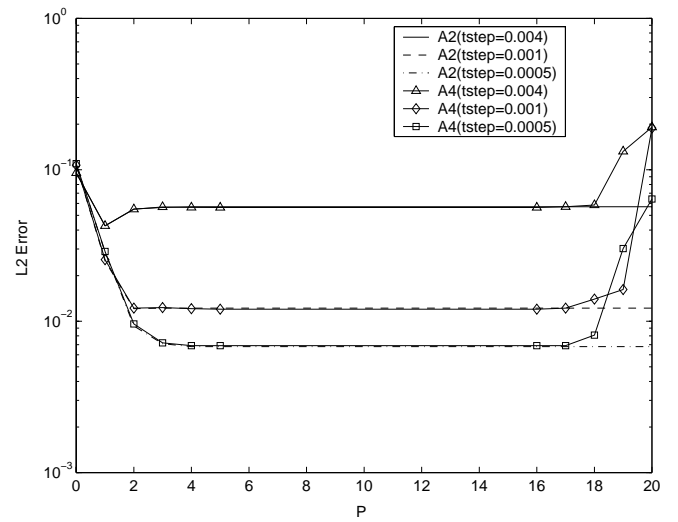


Figure 5. Maximum L_2 error during steady-state measured on the circular artificial boundary Γ using the uniform mesh (Mesh1). Results compared with the direct implementation of the sequence of local radiation boundary conditions $LBC(p)$ with the semi-implicit time integration algorithm, denoted $A4$, compared to an indirect implementation using a Fourier expansion and explicit time-integration as described in (Thompson,1999a; Thompson,2000), denoted $A2$.

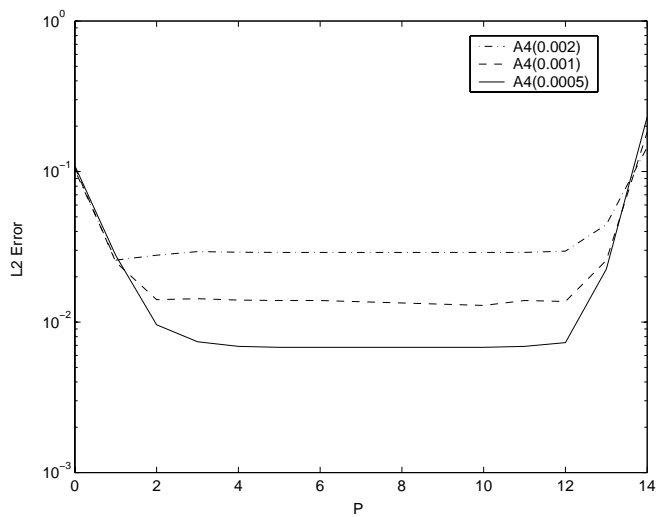
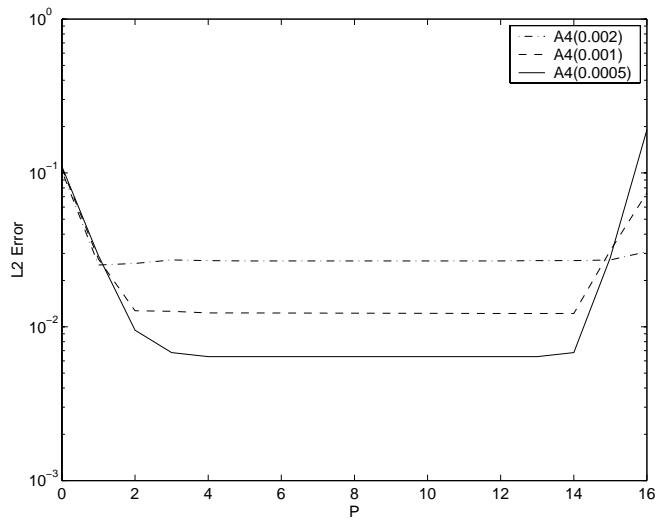


Figure 6. Maximum L_2 error during steady-state using the unstructured meshes (Top) Mesh2, (Bottom) Mesh3. The numbers in the parenthesis indicate the time step size used.